Analysis of crosstalk and field coupling to lossy MTL's in a SPICE environment

Analysis of Crosstalk and Field Coupling to Lossy MTL's in a SPICE Environment

Ivan Maio, Flavio G. Canavero, *Member, IEEE,* and Bruno Dilecce

Abstract—**This paper proposes a circuit model for lossy multiconductor transmission lines (MTL's) suitable for implementation in modern SPICE simulators, as well as in any simulator supporting differential operators. The model includes the effects of a uniform or nonuniform disturbing field illuminating the line and is especially devised for the transient simulation of electrically long wideband interconnects with frequency dependent per-unit-length parameters. The MTL is characterized by its transient matched scattering responses, which are computed including both dc and skin losses by means of a specific algorithm for the inversion of the Laplace Transform. The line characteristics are then represented in terms of differential operators and ideal delays to improve the numerical efficiency and to simplify the coding of the model in existing simulators. The model can be successfully applied to many kinds of interconnects ranging from micrometric high-resistivity metallizations to low-loss PCB's and cables, and can be considered a practical extension of the widely appreciated lossless MTL SPICE model, of which maintains the simplicity and efficiency.**

I. Introduction

HIGH speed requirements in modern technology of analog and digital circuits have greatly emphasized the importance of signal integrity and electromagnetic compatibility (EMC) problems in electronic devices and systems.

Thus, the analysis of the influence of both the external electromagnetic fields and the parasitic phenomena on signal propagation along interconnecting networks is now a major design issue at any level of circuit integration.

This, in turn, calls for accurate and fast techniques of interconnect modeling which must be suitable for time domain simulations, in order to cope with the strong nonlinearities that usually affect the end loads.

Moreover, losses and skin effect have to be taken into account since they are now a relevant issue in many applications, and the distributed effects of the electromagnetic field to line coupling should be included in order to assess the influence of both distant and nearby electromagnetic interference (EMI) sources on the overall system performance.

Finally, the possibility of an easy implementation in standard circuit analysis programs, both at macromodel (subcircuit) and at primitive (C-code) level, should be fulfilled so that designers could find the interconnects models in the simulation environment they usually employ, where a variety of linear and nonlinear circuit elements and several device model libraries are already available.

In the past few years, a great deal of work has been done to address the problem of modeling the interconnecting networks by regarding them as multiconductor transmission lines. Comparisons to full wave numerical approaches and to experimental results have pointed out the validity and the effectiveness of the "transmission line" model for a large number of practical configurations [1]. The analysis of terminated multiconductor transmission lines (MTL's) was treated in many papers, considering both the frequency-domain and the time-domain solution [2], [3]. Correspondingly, several SPICE models for lossy MTL's have been developed, where constant (dc or fixed frequency) losses [4], [5] as well as frequency dependent losses [6], [7]) where taken into account.

SPICE models for MTL's illuminated by an external field have been developed too: The plane wave coupling to lossless homogeneous MTL's was considered in [8]; a model for plane wave interference on lossless non homogeneous MTL's was devised in [9]; the case of a nonuniform field illuminating a lossless homogeneous MTL was also presented in [10]. In all these formulations, the distributed nature of the field-to-line coupling is rigorously taken into account. The effect of the disturbing field is accounted for by lumped equivalent generators.

The inclusion of losses in the simulation of illuminated MTL's, possibly within a standard simulation environment like SPICE, is evidently important, as also recognized in the conclusion of [9]. In this paper, we accomplish this task by generalizing a SPICE model for lossy MTL's with source terms equivalent to the (uniform or nonuniform) field illuminating the interconnect. The model describes a single MTL and is devised for electrically long interconnects (i.e., with a relevant time-delay) with wide bandwidth (i.e., low losses) and, possibly, frequency dependent per-unit-length (p.u.l.) internal impedance. Such interconnects are the most critical ones for both signal integrity and susceptibility to external fields, and they must be effectively handled by any model taking into account the effects of disturbing fields. On the other hand, the time-domain characterization of these interconnects is particularly difficult and requires a specific approach, for their responses have stiff behaviors [11].

In order to handle effectively this kind of interconnects, the MTL is characterized by the matched scattering parameters, which have a simple time evolution, yield simple expression of external field equivalent sources, and lead to the generalized equivalent circuit of Branin type [12]. The time evolution of

Manuscript received May 24, 1995; revised February 5, 1996..

I. Maio and F. G. Canavero are with the Dipartimento di Elettronica, Politecnico, Torino, Italy.

B. Dilecce is with the Centro Ricerche Fiat, Orbassano, Italy.

Publisher Item Identifier S 0018-9375(96)06291-6.

the scattering parameters are computed by a suitable algorithm for the inversion of Laplace transform [13], which offers error control and performs well also for low-loss interconnects with frequency dependent p.u.l. parameters. Finally, to facilitate the SPICE implementation of the model and to improve the numerical efficiency of simulations, we represent the scattering time characteristics by ideal time delays and differential operators. We generate the differential characteristics following the time-domain fitting approach of [14], which, although less used than the frequency-domain approach, offers interesting advantages for the problem at hand.

In fact, the time-domain fitting approach, combined with the numerical inversion of the Laplace Transform, allows to treat frequency dependent p.u.l. parameters without any specific care. It yields the result in the pole-residue form and, though less efficient than other fitting methods, copes very well with the stiffness of the transient scattering responses of low-loss lines, leading to a practical approximation of relatively low order. Besides, in the time-domain fitting approach, the influence of the error of the MTL characteristics on the transient simulation is easier to estimate, allowing a direct tradeoff between the order of the differential characteristics (i.e., their numerical cost) and the accuracy required.

In dealing with differential models of MTL's, it is interesting to note that the proposed model is devoted to electrically long lines and in no way can represent more than a MTL as a single linear multiport. When the time delays of interconnects are not so relevant, the asymptotic waveform evaluation (AWE) method [15] is the most effective to generate the differential characteristics of linear circuits containing MTL's; besides, it can represent networks containing several MTL's as a single multiport. However, when the time delay of an interconnect becomes relevant, accuracy requirements impose the extraction of its time delay and its modeling as a single linear element (see Section 5.6 of [15]). In this case, the AWE approach can still be applied to obtain the differential characteristics of the single MTL (e.g., [16], [23]), but the time-domain approach adopted here can be considered an interesting alternative.

In Section II, we review the transient scattering equation of terminated MTL's, leading to the well known generalized Branin's equivalent circuit, and complete them with field coupling equivalent sources. The evaluation and differential representation of the MTL characteristics is discussed in Section III and, finally, examples of field coupling and crosstalk simulations for a realistic multiconductor interconnect are given in Section IV.

II. Transient Scattering Equations of the Illuminated MTL

The problem considered in this paper is defined in Fig. 1, where a terminated multiconductor interconnect illuminated by an external field is represented. In Fig. 1, v_{pq} and i_{pq} ($p = 1, 2$ and $q = 1, \cdots, N$ throughout the paper) represent the voltages and currents at the MTL ends, respectively, whereas the excitation is provided by the sources included

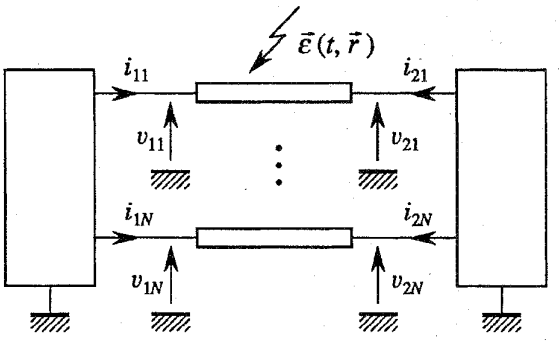

Fig. 1. Terminated MTL illuminated by an external field $\vec{\mathcal{E}}$. The multiport loads can contain linear and nonlinear lumped elements. The electrical variables (voltages and currents) of the MTL ports are also indicated.

into the termination networks (linear or nonlinear) and by the impinging field $\vec{\mathcal{E}}(t, \vec{r})$.

In the analysis of MTL problems, it is convenient to arrange variables in vector form. For the problem of Fig. 1, the vector variables are obtained by collecting the scalar quantities of the same type defined in the same transverse section on the $(N + 1)$ conductors. For example, the vector of currents at line end no. 1 is $\mathbf{i}_1 = (i_{11}, \cdots, i_{1N})^T$, and the vector of voltages at line end no. 2 is $\mathbf{v}_2 = (v_{21}, \cdots, v_{2N})^T$ (^{T} means matrix transposition). It is also useful to introduce the following matrices and functions (s is the complex frequency, and upper and lower case letters indicate Laplace transform pairs): $\overline{\mathbf{Z}} = \mathbf{R}(s) + s\mathbf{L}$ and $\overline{\mathbf{Y}} = \mathbf{G}(s) + s\mathbf{C}$ are the p.u.l. line impedance and admittance matrices, respectively (the inductive and capacitive frequency dependence is included into $\mathbf{R}$ and $\mathbf{G}$, respectively); $\mathbf{M}_v(s)$ and $\mathbf{M}_i(s) = \mathbf{M}_v^{-1^T}$ are the matrices of voltage and current modal profiles, respectively: they are solutions of the eigenvalue problems

$$\begin{aligned} \overline{\mathbf{Z}}\,\overline{\mathbf{Y}}\mathbf{M}_v &= \mathbf{M}_v\mathbf{\Lambda}^2 \\ \overline{\mathbf{Y}}\,\overline{\mathbf{Z}}\mathbf{M}_i &= \mathbf{M}_i\mathbf{\Lambda}^2 \end{aligned} \tag{1}$$

where $\mathbf{\Lambda} = \text{diag}\{\Lambda_k\}$ is the matrix collecting the modal wavenumbers Λ_k; $\mathbf{Y}$ is the line characteristic admittance, given by $\mathbf{Y} = \overline{\mathbf{Y}}\mathbf{M}_v\mathbf{\Lambda}^{-1}\mathbf{M}_v^{-1} = \mathbf{M}_i\mathbf{Y}_m\mathbf{M}_v^{-1}$, where $\mathbf{Y}_m = \text{diag}\{Y_{mk}\}$ is the matrix of modal characteristic admittances. A detailed justification of the results summarized above can be found, with slightly different notations, in [12].

In order to obtain an effective transient formulation of the problem, we describe the MTL response in terms of matched current wave variables, defined by

$$\begin{aligned} \mathbf{A}_p &= \tfrac{1}{2}(\mathbf{Y}\mathbf{V}_p + \mathbf{I}_p), \\ \mathbf{B}_p &= \tfrac{1}{2}(\mathbf{Y}\mathbf{V}_p - \mathbf{I}_p). \end{aligned} \tag{2}$$

The line characteristics relating the wave variables have a simple transient evolution and yield simple field coupling equivalent sources (see Sections II-A and B). In particular, we resort to current wave variables because they are defined for $s = 0$ also for RLC MTL's [it is easy to show that, for RLC MTL's, $\mathbf{Y}(0) = 0$]. This implies that our formulation is suitable also for predicting the dc steady state of the RLC

lines which constitute an important class of interconnects. The line equations for the current waves are

$$\begin{aligned}\mathbf{B}_1 &= \mathbf{H}(\mathcal{L})\mathbf{A}_2 + \overline{\mathbf{B}}_{f1}\\ \mathbf{B}_2 &= \mathbf{H}(\mathcal{L})\mathbf{A}_1 + \overline{\mathbf{B}}_{f2}\end{aligned} \tag{3}$$

where $\mathcal{L}$ is the line length, $\mathbf{H}$ is the matched transmission matrix for current waves [17], i.e., $\mathbf{H}(z) = \mathbf{M}_i(s)\,\mathrm{diag}\,\{\exp(-\Lambda_k z)\}\mathbf{M}_i^{-1}(s)$ (z is the coordinate along the line, originating at end no. 1), and $\overline{\mathbf{B}}_{fp}$ are the equivalent current wave sources accounting for the disturbing field. The equivalent sources are given by [17]

$$\begin{aligned}\overline{\mathbf{B}}_{f1} &= -\tfrac{1}{2}\int_0^{\mathcal{L}} \mathbf{H}(z)[\mathbf{Y}\overline{\mathbf{E}}(s,z) - \overline{\mathbf{I}}(s,z)]\,dz\\ \overline{\mathbf{B}}_{f2} &= \tfrac{1}{2}\int_0^{\mathcal{L}} \mathbf{H}(\mathcal{L}-z)[\mathbf{Y}\overline{\mathbf{E}}(s,z) + \overline{\mathbf{I}}(s,z)]\,dz\end{aligned} \tag{4}$$

where $\overline{\mathbf{E}}(s,z)$ and $\overline{\mathbf{I}}(s,z)$ are the distributions of series-voltage and shunt-current generators induced along the line conductors by the external field. The existence and the expressions of these generators depend on the field coupling formulation adopted: they are both present in case of a "balanced" formulation [18], while the current source is absent in case of the "electric field" formulation [19], and the voltage source is omitted by the "magnetic field" formulation [20]. Compensation lumped series-voltage (shunt-current) generators must also be connected at the line ends in the case of electric (magnetic) field formulation.

In this formulation, no assumptions are made about the exciting field, which can be nonuniform. Such a case is handled by deriving the values of the field in a suitable number of points distributed along the relevant integration paths from the assumed knowledge of the field in the space surrounding the line. A piecewise linear interpolation of the field along the line is then adopted to avoid numerical integration, and has proven to be a good tradeoff between precision and simplicity of implementation [10].

A. Plane Wave Impinging Field

In the important case of a plane wave interfering field, the spatial integration of the field-coupling sources (4) can be carried out analytically. For the "electric field" formulation [19] [i.e., $\overline{E}_q(s,z) \propto \mathcal{E}_z$ and $\overline{I}_q(s,z) = 0$], the explicit expressions of $\overline{\mathbf{B}}_{fp}$ are given in [21], where a split version of these sources is also proposed. The final expressions of the split equivalent sources, which offer numerical advantages in the transient analysis of lossy lines, are

$$\begin{aligned}\mathbf{B}_1 &= \mathbf{H}(\mathcal{L})(\mathbf{A}_2 + \mathbf{A}_{f2}) + \mathbf{B}_{f1}\\ \mathbf{B}_2 &= \mathbf{H}(\mathcal{L})(\mathbf{A}_1 + \mathbf{A}_{f1}) + \mathbf{B}_{f2}\end{aligned} \tag{5}$$

$$\begin{aligned}\begin{pmatrix}\mathbf{B}\\ \mathbf{A}\end{pmatrix}_{f1} &= -\frac{1}{2}\mathbf{M}_i(s)\,\mathrm{diag}\left\{\frac{Y_{mk}}{\Lambda_k\left(\begin{smallmatrix}+\\ -\end{smallmatrix}\right)\Lambda_0}\right\}\\ &\quad\cdot \mathbf{M}_v^{-1}(s)\mathbf{G}(s)E(s),\\ \begin{pmatrix}\mathbf{B}\\ \mathbf{A}\end{pmatrix}_{f2} &= -\begin{pmatrix}\mathbf{A}\\ \mathbf{B}\end{pmatrix}_{f1} e^{\Lambda_0\mathcal{L}}\end{aligned} \tag{6}$$

where $E(s)$ is the spectrum of the interfering signal, $\Lambda_0 = (s/v_0)\hat{n}\cdot\hat{z}$ is the wavenumber of the plane wave in the z direction ($\hat{n}$, $\hat{z}$ are wave propagation and z-direction unit vectors, respectively, v_0 is the speed of light in the dielectric medium), and $\mathbf{G}(s)$ is a vector of transfer functions [21].

B. SPICE Equivalent Circuit

The MTL description is completed by the equations converting current wave variables into voltages and currents, and vice versa

$$\begin{aligned}\mathbf{I}_p &= \mathbf{Y}\mathbf{V}_p - 2\mathbf{B}_p,\\ \mathbf{A}_p &= \mathbf{I}_p + \mathbf{B}_p.\end{aligned} \tag{7}$$

These equations, along with (3) or (5) admit the simple circuit interpretation known as generalized Branin's equivalent circuit [22], and allow the SPICE analysis of the problem of Fig. 1.

In view of the transient simulation, it is useful to cast the MTL equations and their equivalent circuit in terms of modal variables defined by $\mathbf{V}_{mp} = \mathbf{M}_v(s)\mathbf{V}_p$ and $\mathbf{I}_{mp} = \mathbf{M}_i(s)\mathbf{I}_p$. The decoupled modal line equations are

$$\begin{aligned}\mathbf{B}_{m1} &= \mathrm{diag}\,\{H_{mk}\}(\mathbf{A}_{m2} + \mathbf{A}_{m02}) + \mathbf{B}_{m01}\\ \mathbf{B}_{m2} &= \mathrm{diag}\,\{H_{mk}\}(\mathbf{A}_{m1} + \mathbf{A}_{m01}) + \mathbf{B}_{m02}\end{aligned} \tag{8}$$

$$\begin{aligned}\mathbf{I}_{mp} &= \mathrm{diag}\,\{Y_{mk}\}\mathbf{V}_{mp} - 2\mathbf{B}_{mp},\\ \mathbf{A}_{mp} &= \mathbf{I}_{mp} + \mathbf{B}_{mp}\end{aligned} \tag{9}$$

where $H_{mk} = \exp(-\Lambda_k\mathcal{L})$, $\mathbf{A}_{mp} = \mathbf{M}_i^{-1}\mathbf{A}_p$, $\mathbf{B}_{mp} = \mathbf{M}_i^{-1}\mathbf{B}_p$, and the sources $\mathbf{A}_{m0p}$ and $\mathbf{B}_{m0p}$ are $\left(\begin{smallmatrix}\mathbf{A}\\ \mathbf{B}\end{smallmatrix}\right)_{m0p} = \mathbf{M}_i^{-1}\left(\begin{smallmatrix}\mathbf{A}\\ \mathbf{B}\end{smallmatrix}\right)_{0p}$, with $\mathbf{A}_{0p} = 0$ and $\mathbf{B}_{0p} = \overline{\mathbf{B}}_{fp}$ for a general excitation, and $\mathbf{A}_{0p} = \mathbf{A}_{fp}$, $\mathbf{B}_{0p} = \mathbf{B}_{fp}$ for a plane wave excitation. The corresponding MTL Branin's equivalent circuit uses modal transformers and is shown in Fig. 2 for the reader's reference.

The line characteristics are equivalently expressed by the operators $\mathbf{H}(s)$ and $\mathbf{Y}(s)$ or by the operators $\mathbf{M}_v(s)$, $\mathrm{diag}\,\{H_{mk}\}$, and $\mathrm{diag}\,\{Y_{mk}\}$ depending on the physical or modal formulation, respectively.

III. MTL Transient Characteristics

The most effective representation of the line characteristics for the integration of the circuit transient equations is the one that uses differential operators. They offer high numerical efficiency and, even more important for an implementation as macromodels, they are directly accepted in the form of differential blocks or rational transfer functions by several members of the family of SPICE simulators. Of course, to exploit the numerical efficiency of differential characteristics, the simulator must compute the transient response of the differential blocks by difference equations and not by numerical convolutions.

Many methods and different network parameters, including the scattering operators $\mathbf{H}$ and $\mathbf{Y}$, have been considered to generate differential characteristics for MTL's. For example, circuit equivalents of simplified $\mathbf{H}(j\omega)$ and $\mathbf{Y}(j\omega)$

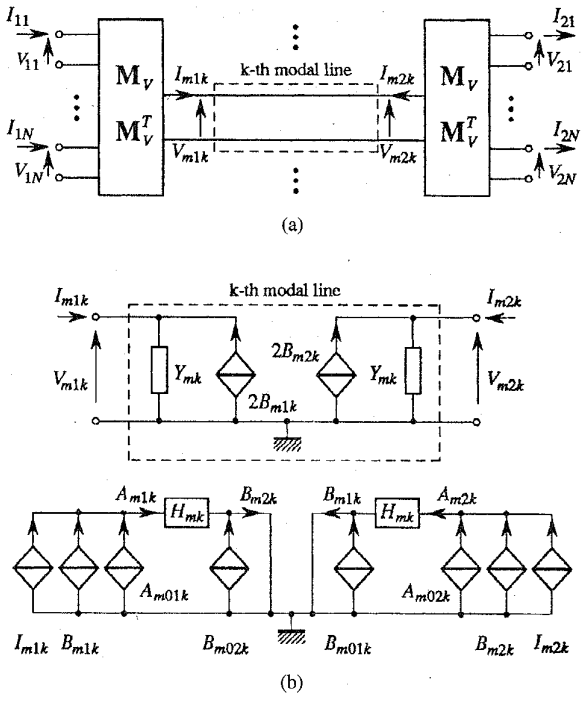

Fig. 2. Generalized Branin's equivalent circuit of the disturbed MTL of Fig. 1. Multiport networks are modal transformers relating physical and modal quantities. The internal sources are explained in the text.

characteristics were used in [5], frequency-domain fitting of characteristics with rational functions by optimization methods and by Padé approximations were considered in [6], [16], and [23], respectively, whereas time-domain fitting of MTL responses with sums of exponential functions was proposed in [14].

Some of these methods were applied also to MTL's with frequency dependent p.u.l. parameters [7], [24], [25], which is particularly important for the modeling of wideband interconnects of macroscopic size. In fact, the time response of these structures is dominated by skin losses [11] and cannot be correctly described without considering the frequency dependence of the p.u.l. internal impedance.

In this paper, we explore the time-domain method of [14] in combination with the numerical inversion of the Laplace Transformation to generate the differential characteristics of MTL with frequency dependent p.u.l. parameters. To the author's knowledge, the time-domain fitting method has received less attention than others, probably owing to the difficulty of computing reliable MTL time responses at low cost. The algorithm for the inversion of the Laplace Transform proposed in [13] allows the effective evaluations of the MTL transient responses $\mathbf{h} = \mathcal{L}^{-1}[\mathbf{H}]$ and $\mathbf{y} = \mathcal{L}^{-1}[\mathbf{Y}]$ or $\mathbf{m}_v = \mathcal{L}^{-1}[\mathbf{M}_v]$, $\mathbf{h}_m = \mathcal{L}^{-1}[\text{diag}\{H_{mk}\}]$, and $\mathbf{y}_m = \mathcal{L}^{-1}[\mathbf{Y}_m]$ also in the difficult case of low-loss (i.e., wideband) and frequency dependent p.u.l. parameters. Hence, it becomes interesting to fit these responses with sums of exponential functions.

When the differential representation of the line characteristics is used, the modal formulation of Section II-B is more efficient and, therefore, the fitting of $\mathbf{m}_v$, $\mathbf{h}_m$, and $\mathbf{y}_m$ is preferable. Unfortunately, no general results are available for the diagonalization of lossy MTL's with frequency dependent parameters, which means that the properties of $\mathbf{m}_v$, $\mathbf{h}_m$, and $\mathbf{y}_m$ functions are rather unknown and a complete classification of structures for which the time fitting is possible and practical can hardly be done. The simplest way is to experiment with significant examples representing the class of structures of interest. For example, we obtained satisfactory fittings of $\mathbf{m}_v$, $\mathbf{h}_m$, and $\mathbf{y}_m$ for a coaxial cable over a metallic plane, which is a problem with a nearly antidiagonal $\mathbf{R}(s)$ model.

An important class of lossy MTL's, for which the time fitting approach is successful, is composed by the structures with weakly inhomogeneous dielectric and nearly diagonal $\mathbf{R}(s)$ matrices (e.g., planar multistrip structures, wire tapes, and bundles in air). For low losses, the frequency dependence of the modal profile matrix $\mathbf{M}_v(s)$ of these structures is weak and has a negligible effect on the overall time responses $\mathbf{h}$ and $\mathbf{y}$. In fact, in these structures, the change of $\mathbf{M}_v$ occurs at low frequencies and influences $h_{qq'}$ and $y_{qq'}$ only for very long times, where their values are negligible. As a result, fairly well approximated transient characteristics (at least up to a time on the order of $L_{\max}/R_{\max}$, where $L_{\max}$ and $R_{\max}$ are the largest elements of $\mathbf{R}(0)$ and $\mathbf{L}$, respectively) can be obtained by replacing $\mathbf{M}_v(s)$ and $\mathbf{M}_i(s)$ with their value for $s \to \infty$ i.e., in the lossless case. The approximate frequency characteristics for these problems are therefore

$$\begin{aligned}\mathbf{Y}_a &= \mathbf{M}_i(\infty)\mathbf{Y}_m\mathbf{M}_v^{-1}(\infty)\\ &\approx \mathbf{Y}\\ \mathbf{H}_a &= \mathbf{M}_i(\infty)\,\text{diag}\{\exp(-\Lambda_k\mathcal{L})\}\mathbf{M}_i^{-1}(\infty)\\ &\approx \mathbf{H}\end{aligned} \tag{10}$$

and can be validated at negligible cost by comparing time responses $\mathbf{y}_a$ and $\mathbf{h}_a$ with $\mathbf{y}$ and $\mathbf{h}$ computed by numerical inversion of Laplace transform.

When the above approximation holds, the modal transformers of the equivalent circuit of Fig. 2 are replaced with constant modal transformers defined by $\mathbf{M}_v(\infty)$, and the equivalent field coupling sources $\binom{\mathbf{A}}{\mathbf{B}}_{m0p}$ with $\binom{\mathbf{A}}{\mathbf{B}}_{ma0p} = \mathbf{M}_i^{-1}(\infty)\binom{\mathbf{A}}{\mathbf{B}}_{0p}$. Moreover, only the differential representation of h_{mk} and y_{mk} is needed.

Functions h_{mk} and y_{mk} can be successfully fitted with sums of exponential functions because they have a simple evolution and are independent, as they are a solution of a diagonal problem. We carry out the fitting with the following procedure. We select the minimum and maximum time values of interest, $T_{\min}$ and $T_{\max}$, respectively. Time $T_{\min}$ is set by the bandwidth of the driving signals and of the lumped loads, and $T_{\max}$ is the duration of the simulation. Then, we limit the fitting of the line responses to the interval $[T_{\min}, T_{\max}]$ and use the additional condition $\int_0^{T_{\min}} \overline{h}_{mk}(t)\,dt = \int_0^{T_{\min}} h_{mk}(t)\,dt$ to ensure the consistency of the approximation, also when a significant part of the responses falls before $T_{\min}$; the quantity $\overline{h}_{mk}(t)$ represents the fitted impulse response. This simple condition can account for the neglected part of the responses, because the signals transformed by the line operators are approximately constant over a time interval of duration $T_{\min}$.

In order to automatically satisfy this condition and to deal with functions with a smaller dynamic range, it is preferable to fit the step response functions $\int_{T_k}^{t} h_{mk}\,dt'$ and $\int_{0}^{t} y_{mk}\,dt'$, where $T_k = \lim_{s\to\infty} \Lambda_k \mathcal{L}/s$ is the time delay of mode k. The needed reference step responses are still computed by the numerical inversion of the Laplace Transform by simply adding the factor $1/s$ to the frequency characteristics. The fitting of the step responses is then carried out by the least square method varying both the coefficients and the natural frequencies of the exponential functions.

As an example of the above-mentioned procedure, Fig. 3 shows a typical transmission impulse response h_{mk}, compared with two exponential approximations of different order. Logarithmic scales are used for both the function value and the time scale, in order to show both the fast-rising initial peak due to skin losses and the long slower tail controlled by dc losses.

The characterization procedure adopted has interesting advantages for the class of interconnects considered. Although the nonlinear fitting of functions with exponential sums is less efficient than other fitting approaches, it appears fairly adequate to cope with the stiff behavior (fast initial part and slow long-time evolution) of the responses of lossy wideband interconnects [11]. In practice, good approximations of h_{mk} functions over three or four time decades can be obtained by three to six natural frequencies, which allow the fitting of a response in a few seconds of computation. Besides, time-domain fitting is easier than the frequency-domain one, and the error affecting the transient simulation can be directly appreciated, allowing tradeoffs between the needed accuracy and the order (i.e., numerical cost) of the differential representations generated. Finally, the approximation with exponential functions yields the result in pole-residue form, which means that the differential operator is represented by a parallel combination of first or second order differential operators, and is particularly suited for numerical integration. Often, a simple circuit synthesis of the differential representation generated in this way is also possible, allowing to exploit the efficiency of the differential characteristics for those SPICE simulators that handle rational blocks by numerical convolution.

IV. Application

In this section, we concentrate on the SPICE transient simulation of the interference effects in a realistic low-loss nonlinearly loaded interconnect. The aim of the example is to show how a typical EMC simulation problem fits in the simplified description of the previous section and how possible errors arising from lossless models can be avoided at very little additional cost with our approach.

A. Circuit and MTL Structure

The circuit of this example is described in Fig. 4, where an asymmetric three-land PCB, driven and loaded by ECL gates, is exposed to an impinging plane wave with a biexponential time envelope, whose expression is

$$\vec{\mathcal{E}}(t,\vec{r}) = \hat{p}A_e(e^{-t'/t_1} - e^{-t'/t_2}), \quad t' = t - \frac{\hat{n}\cdot\vec{r}}{v_o} \tag{11}$$

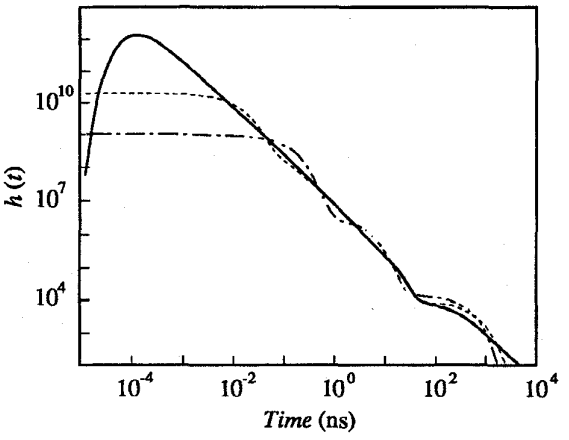

Fig. 3. Example of exponential fitting, in log-log scale, of a matched transmission impulse response. The solid curve is the typical transmission impulse response of a low-loss modal TL, whereas the dashed and dotted curves are exponential approximations in terms of three and five real natural frequencies, respectively.

where $\vec{r}$ is the position vector for the reference frame of Fig. 4, A_e is a dimensional constant related to the electric field strength, and t_1, t_2 are time constants. The reference conductor (ideal) of the MTL coincides with the (y, z) plane and the three lands (of widths w_q, and of thickness d) lie along the z axis at (x_o, y_q), where x_o is the thickness of the dielectric substrate (see Fig. 4 and the parameter values of Table I).

The ECL gates are modeled with the nonlinear simplified models described in [26], which can be readily replaced by more accurate models of commercial devices by the final user.

The transfer functions $\mathbf{G}$ for the distributed voltage generators (6) are obtained from the primary electric field (incident plus reflected) in the stratified dielectric medium i.e.,

$$G_q = 2\sin(\psi)\cos(\theta)x_o\frac{s}{v_o}\left[1 + y_q\sin(\psi)\sin(\theta)\frac{s}{v_o}\right] \tag{12}$$

where the electric field is assumed to be contained in the (y, z) plane, and the approximations allowed by the condition of a slowly varying disturbing field (i.e., $t_{1,2} \gg x_o/v_o,\ y_q/v_o$) are also exploited.

The MTL is assumed of RLC type. The resistance matrix is written in the form $\mathbf{R}(s) = \mathrm{diag}\{R_q\}$ and its elements are approximated as in [27] i.e.,

$$R_q(s) = \frac{R_{\mathrm{dc},q}}{1 - \exp\left\{\dfrac{R_{\mathrm{dc},q}}{R_{o,q}\sqrt{2s}}\right\}} \tag{13}$$

where $R_{\mathrm{dc},q}$ and $R_{o,q}\sqrt{2s}$ are the p.u.l. dc and high-frequency skin effect resistances [28] of the qth copper strip, respectively. This resistance model is one of the simplest available for rectangular conductors, yet is fairly adequate for the considered example, because in the simulation interval considered the line impulse responses are mainly determined by skin losses.

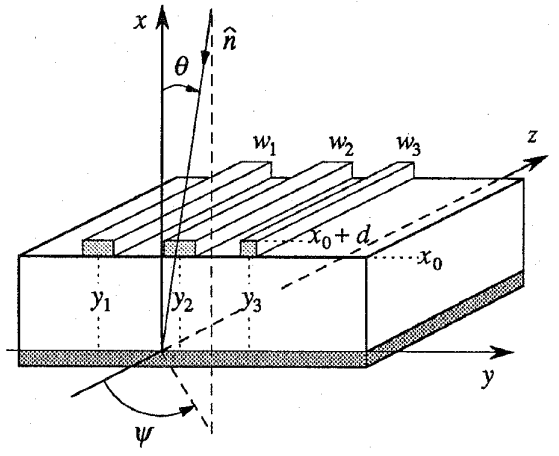

(a)

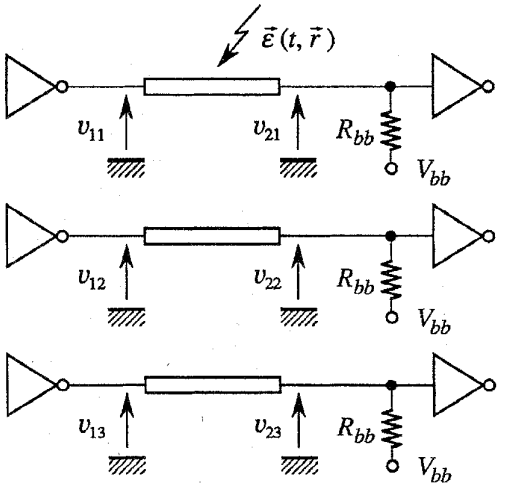

(b)

Fig. 4. Scheme of the application developed in Section IV: (a) the structure of the MTL and its geometrical reference frame used to describe the impinging field (parameter values are in Table I), and (b) the MTL connected to ECL gates and their pull-down networks.

TABLE I
PARAMETER VALUES OF THE EXAMPLE

Interfering Plane Wave Parameters	
A_e	-10^3 V/m
t_1, t_2	10^{-8}, 10^{-9} s
θ	45°
ψ	60°
$\hat{p} \cdot \hat{x}$	0
Geometrical and Electrical Characteristics of the Line	
$\mathcal{L}$	0.2 m
y_1, y_2, y_3	-300, 0, 280 μm
x_o	625 μm
w_1, w_2, w_3	100, 100, 60 μm
d	30 μm
ϵ_r substrate	4.7
σ strip	5.6×10^7 m$^{-1}\,\Omega^{-1}$
Circuit Parameters	
R_{bb}	600 Ω
V_{bb}	$-2V$

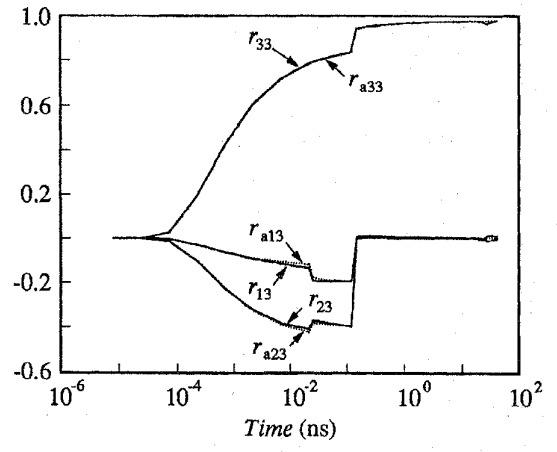

(a)

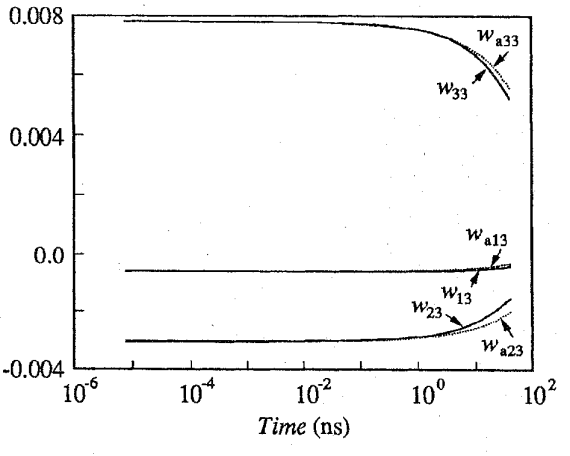

(b)

Fig. 5. Some of the step response functions of the application developed in Section IV: (a) current-wave matched transmission step responses, and (b) admittance step responses. The solid curves refer to the exact functions, and the dotted ones are obtained by assuming frequency-independent modal profiles. Logarithmic scales are used for the time variable, and in (a) the time origin is located at the arrival of the fastest travelling mode ($t = 1.005$ ns).

B. Transient Characteristics

Some of the time characteristics computed by numerical inverse Laplace transformation for the structure of this example are shown in Fig. 5. Specifically, Fig. 5 shows $r_{q3} = \int h_{q3}\,dt'$, $w_{q3} = \int y_{q3}\,dt'$, $r_{aq3} = \int h_{aq3}\,dt'$, and $w_{aq3} = \int y_{aq3}\,dt'$. From the physical point of view, the r_{q3} (w_{q3}) functions are the current responses of the matched line at end no. 2 (no. 1) to a step current wave injected at end no. 1 of conductor no. 3. In order to show the step response evolutions over a long time interval Fig. 5 has logarithmic time scales, and the time scale for r_{q3} and r_{aq3} originates at the delay of the fastest travelling mode. The two knees in r_{q3} and r_{aq3} correspond to the onset of the contributions of the two slower modes, whereas the unphysical segmentation of the initial part of these curves comes from the poor sampling adopted at subpicosecond times (which are irrelevant for this analysis). As expected, the approximate responses deduced

from constant modal profiles are barely distinguishable from the exact ones up to large time values, and this justifies the use of the simplified model of Section III.

The comparison of the three modal step responses highlights the different behavior of the three modes. The fastest travelling mode has an odd structure and experiences the highest losses (slow growth), whereas the other two modes have an even structure and experience lesser losses. As a result, even in a structure with p.u.l. resistance as low as in this example, some mode can experience considerable losses, possibly leading to unexpected degradations of the bus signals.

The modal admittances and transmission responses have a fairly smooth evolution, allowing us to obtain good exponential fittings over the time interval [10 ps, 50 ns] with two real natural frequencies for the admittances and four real natural frequencies for the transmission responses.

The transient evolution of field coupling equivalent sources is obtained by inverse transformation of (6). Owing to the small distortion effect of the overall transfer function for the input spectrum E, the transient equivalent sources are simply slightly distorted replicas of the impinging biexponential [17].

C. Numerical Results

The far end voltages obtained by our model for the structure of Fig. 4(a) with perfectly matched terminations and an ideal step voltage applied to end no. 1 of land no. 3 are shown in Fig. 6, along with the responses computed by the lossless SPICE model and the reference transmission step responses used to obtain the differential characteristics. It should be noted that the reference responses are different from those of Fig. 5(a), because the latter are current waves transmission step responses. The accuracy of the approximate differential characteristics adopted, as well as the accuracy of their implementation in the SPICE model, is evidenced by the good agreement between the reference and the SPICE responses. The comparison with the lossless responses, on the other hand, shows how losses mainly affect the direct transmission along land no. 3. In fact, the relative contributions of the modes to τ_{33}, which can be appreciated from the steps of Fig. 5(a), point out the dominance of the most lossy mode in the direct signal transmission along land no. 3.

An example of simulated far end signals for the complete circuit of Fig. 4(b) and for an HIGH logic pulse applied by the gate driving land no. 3 is shown in Fig. 7. The pulse starts at $t = 0.1$ ns, lasts 1 ns and has typical rise and fall times of 100 ps; no external field is applied. The curves of Fig. 7 represent the received voltage waveforms v_{2q} obtained by our model and by the SPICE lossless model. The widest difference between lossy and lossless simulations occurs in the waveform of v_{23}, which, in this example, is the response affected by the largest contribution of the most lossy mode [Fig. 5(a)]. Of course, the departure of the lossy curve v_{23} from the lossless one grows with the order of the reflections, reminding the importance of the effects of even moderate losses in mismatched and in cascaded interconnects.

The numerical efficiency of our approach is supported by the short simulation times obtained, always comparable with

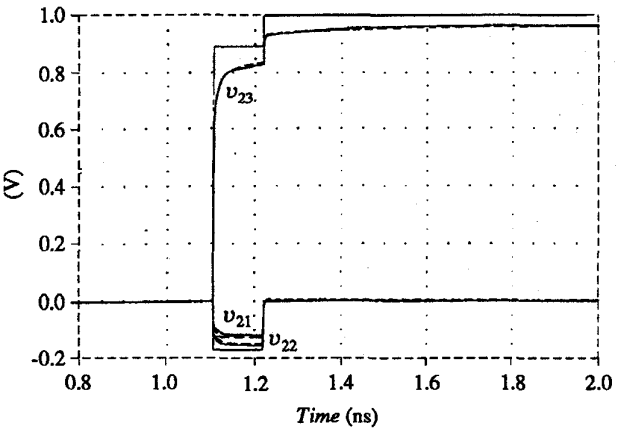

Fig. 6. Comparison of the responses v_{2q} of the structure of Fig. 4(a) when an ideal voltage step is applied to end no. 1 of land no. 3 and matched terminations are used. The staircase and the solid curves are simulated by the SPICE lossless model and by our SPICE lossy model, respectively. The dashed curves are reference responses used to generate the differential characteristics of the lossy model.

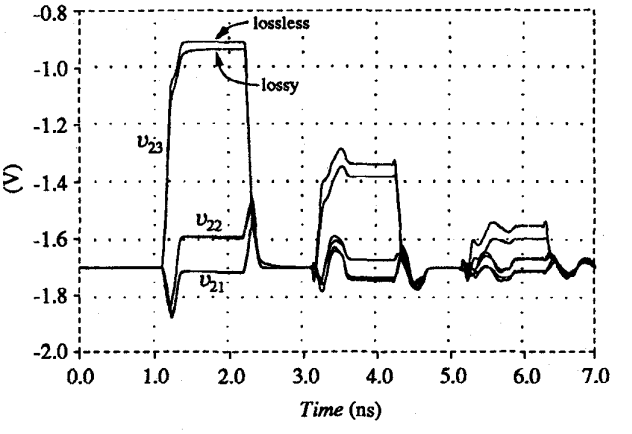

Fig. 7. Simulated voltage waveform at the far end of the circuit of Fig. 4(b), when the inverter driving land no. 3 applies a HIGH logical pulse of 1 ns. Both the voltages v_{2q} obtained with the SPICE lossless model and the proposed model are shown. A significant difference is obtained for the v_{23} response, which, in the example developed, experiences the highest losses. The lossy v_{23} curve is the one with the lowest level, and deviates from the lossless result as far as the order of the reflections grows.

those of the lossless model. For example, the curves of Fig. 7 require approximately 40 s for the lossy case and 30 s for the lossless case on a 486 PC @ 66 MHz. Besides, the lossy model shows stability properties even better than expected, offering troubleless runs also in those cases where the lossless model leads to integration problems.

The effects of the external disturbing field (whose parameters are given in Table I) on the circuit of Fig. 4(b) can be appreciated from the time evolution of the end line voltages shown in Fig. 8. In this case, the logic gates do not change state and the bus lines are kept at a voltage corresponding to the LOW logical state. The excitation of the three lands is almost the same, since the structure is narrow compared to the wavelengths of the impinging field. Also, the shape of the waveforms induced at the line ends can be easily interpreted in

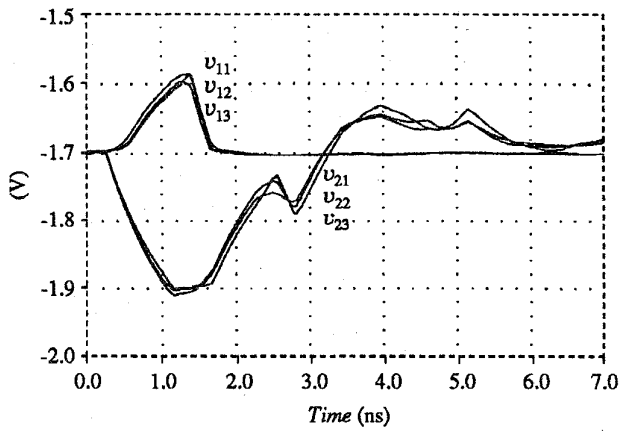

Fig. 8. Transient far end voltages v_{2q} obtained for the circuit of Fig. 4(b) when the biexponential plane wave field of Table I illuminates the MTL and the lands are in the LOW logical state. The interpretation of the waveforms is explained in the text.

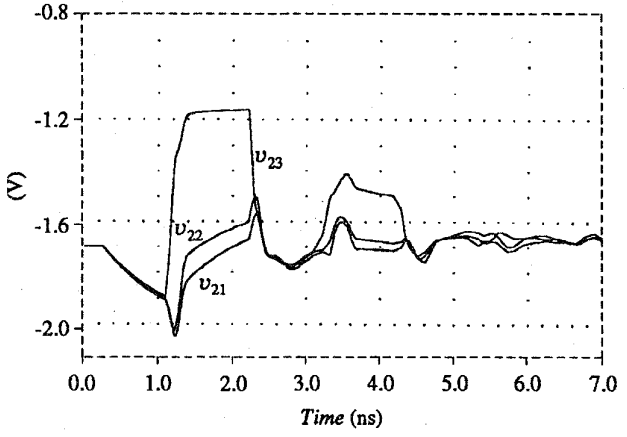

Fig. 9. Transient far end voltages v_{2q} obtained by considering both the internal excitation (a HIGH logical pulse on land no. 3 as in Fig. 7) and an impinging biexponential field (as in Fig. 8). In this case, the disturbing field causes a transmission error, since the received pulse does not reach the HIGH logical level.

terms of the $\mathbf{b}_{fp}$ and $\mathbf{a}_{fp}$ sources, which are slightly distorted replicas of the biexponential signal. For example, v_{2q} has a decreasing edge due to b_{f2q}, lasting up to the arrival of a_{f1q}, which has nearly the same shape and opposite sign. The straight long time part of the near end noise is due to the clamping effects of the gate outputs characteristics, which show a small resistance for voltages lower than the LOW logical voltage.

Finally, Fig. 9 shows the simulation of the signal transmission considered in Fig. 7 in the presence of the disturbing field used to produce Fig. 8. In this example, the external interference corrupts the pulse reaching the receiving end, causing a transmission error.

The simulations of Figs. 8 and 9 require approximately 30 and 50 s on a 486 PC @ 66 MHz, respectively. They demonstrate how realistic signal integrity problems can be analyzed in their complete form, with little programming and at a computational cost that is affordable also for large structures.

V. Conclusions

This paper presents a simple SPICE model for the transient and ac simulation of multiconductor interconnects, possibly illuminated by an external field. Besides exploiting all the advantages of the SPICE environment, the model makes effective use of the most efficient approach to the transient simulation of MTL's. In this formulation, the line characteristics are expressed in terms of differential representations of its matched transient scattering parameters, which are computed by numerical Laplace inversion of the frequency characteristics, and take into account the frequency dependence of the p.u.l. parameters (possibly given in numerical form). For any simulation problem, the order of the line differential characteristics can be kept as low as desired, by representing only the parts of the impulse responses affecting the final result. Moreover, since the differential operator is accepted as a standard device by many present SPICE simulators, the line model based on differential characteristics can be easily implemented without any C-code programming.

As a result, the present approach allows the introduction of losses and dispersion in the SPICE analysis of circuits with "long" interconnects (possibly affected by field coupling) with little programming and inexpensive computations. Low-loss (wideband) and, of course, high-loss interconnects are handled in the proposed framework with the simplicity and the cost of the widely appreciated lossless MTL SPICE model.

Acknowledgment

The authors would like to thank F. Muzio for his help in the coding work and L. Brino for providing the line drawings. I. Maio wishes to thank Prof. M. Biey for insightful discussions on SPICE simulators.

References

[1] C. R. Paul and D. F. Herrick, "Coupling of electromagnetic fields to transmission lines," in *Proc. 1982 IEEE Int. Symp. EMC,* Santa Clara, CA, Sept. 1982.
[2] Special issue on simulation, modeling and electrical design of high-speed and high-density interconnects, W. M. Dai, Ed., *IEEE Trans. Circ. Syst.—I,* vol. 39, Nov. 1992.
[3] Special issue on high-speed interconnects, Nakhla and Q. J. Zhang, Eds., *Int. J. Analog Integr. Circ. Sig. Process.,* vol. 5, no. 1, Jan. 1994.
[4] N. Orhanovic, V. K. Tripathi, and P. Wang, "Time domain simulation of uniform and nonuniform multiconductor transmission lines by the method of characteristics," *IEEE Int. Microwave Symp. Dig.,* pp. 1191–1194, May 1990.
[5] K. H. Wirth, "New model for time domain simulation of lossy coupled lines," *Electron. Lett.,* vol. 26, pp. 1723–1724, Sept. 1990.
[6] F. Y. Chang and O. Wing, "Transient simulation of lossy coupled transmission lines characterized with frequency-dependent parameters," *Int. J. High Speed Electron.,* vol. 2, pp. 111–145, 1991.
[7] Q. Yu and O. Wing, "Computational models of transmission lines with skin effects and dielectric loss," *IEEE Trans. CAS—I,* vol. 41, pp. 107–118, Feb. 1994.
[8] B. Dilecce, L. Isnardi, D. Labate, and F. G. Canavero, "Exact SPICE model of field coupling to multiconductor transmission lines," in *Proc. 1994 Int. Symp. EMC,* Sendai, Japan, May 1994, pp. 12–15.
[9] C. R. Paul, "A SPICE model for multiconductor transmission line excited by an incident electromagnetic field," *IEEE Trans. Electromag. Compat.,* vol. 36, pp. 342–354, Nov. 1994.
[10] F. Muzio, B. Dilecce, A. Gonano, and F. Canavero, "SPICE analysis of field coupling to multiconductor transmission lines," in *Proc. Int. Symp. EMC, ROMA,* Roma, Italy, Sept. 13–16, 1994, pp. 386–389.

[11] I. Maio and F. Canavero, "Modeling of line losses and dispersion effects for signal integrity simulation," in *Proc. 11th Int. Zurich Symp. EMC,* Mar. 1995, pp. 197–202.
[12] C. R. Paul, *Analysis of Multiconductor Transmission Lines.* New York: Wiley Interscience, 1994.
[13] T. Hosono, "Numerical inversion of Laplace transform and some applications to wave optics," *Radio Sci.,* vol. 16, pp. 1015–1019, Nov. 1981.
[14] A. Semlyen and H. Dabuleanu, "Fast and accurate switching transient calculations on transmission lines with ground return using recursive convolution," *IEEE Trans. Power App. Syst.,* vol. PAS94, pp. 561–571, Mar. 1975.
[15] E. Chiprout and M. Nakhla, *Asymptotic Waveform Evaluation.* Boston: Kluwer Academic, 1994.
[16] J. E. Bracken, V. Raghavan, and R. A. Rohrer, "Interconnect simulation with asymptotic waveform evaluation (AWE)," *IEEE Trans CAS—I,* vol. 39, pp. 869–878, Nov. 1992.
[17] I. Maio and F. Canavero, "Field coupling and crosstalk in distributed networks with nonlinear loads," *IEEE Trans. Electromag. Compat.,* vol. 37, pp. 599–606, Nov. 1995.
[18] C. D. Taylor, R. S. Satterwhite, and C. W. Harrison, Jr., "The response of a terminated two wire transmission line excited by a nonuniform electromagnetic field," *IEEE Trans. Antennas Propagat.,* vol. AP-13, pp. 987–989, Nov. 1965.
[19] A. K. Agrawal, H. J. Price, and S. H. Gurbaxani, "Transient response of multiconductor transmission lines excited by a nonuniform electromagnetic field," *IEEE Trans. Electromag. Compat.,* vol. EMC-22, pp. 119–129, May 1980.
[20] F. Rachidi, "Formulation of field to transmission line coupling equations in terms of magnetic excitation field," *IEEE Trans. Electromag. Compat.,* vol. 35, pp. 404–407, Aug. 1993.
[21] I. Maio and F. Canavero, "Line models for transient interconnect simulation," in *Proc. IEEE MTT-S Europ. Top. Congress,* Turin, Italy, Nov. 1994, pp. 101–106.
[22] C. R. Paul, *Introduction to Electromagnetic Compatibility.* New York: Wiley Interscience, 1994.
[23] S. Lin and E. S. Kuh, "Transient simulation of lossy interconnects based on the recursive convolution formulation," *IEEE Trans. Circuits Syst.—I,* vol. 39, pp. 879–892, Nov. 1992.
[24] L. Marti, "Simulation of transients in underground cables with frequency-dependent modal transformation matrices," *IEEE Trans. Power Delivery,* vol. 3, pp. 1099–1110, July 1988.
[25] R. Khazaka, E. Chiprout, M. Nakhla, and Q. J. Zhang, "Analysis of high-speed interconnects with frequency dependent parameters," in *Proc. 11th Int. Zurich Symp. EMC,* Mar. 1995, pp. 203–208.
[26] S. Rosenstark, *Transmission Lines in Computer Engineering.* New York: McGraw-Hill, 1994.
[27] Eo and W. R. Einsenstadt, "High-speed VLSI interconnect modeling based on S-parameter measurements," *IEEE Trans. Components Hybrids Manufact. Technol.,* vol. 16, pp. 555–562, Aug. 1993.
[28] R. K. Hoffmann, *Handbook of Microwave Integrated Circuits.* CA: Artech House, 1987, ch. 6.

Ivan Maio received both the Laurea degree and the Ph.D. degree in electronic engineering from the Politecnico di Torino, Italy in 1985 and 1989, respectively.

He is currently with the Department of Electronics at the Politecnico di Torino as a Researcher. His main areas of interest are in nonlinear and distributed circuits and in electromagnetic compatibility.

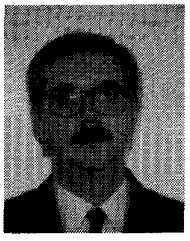

Flavio G. Canavero (M'90) received the Laurea degree in electronic engineering from the Polytechnic of Turin, Italy, and the Ph.D. degree from the Georgia Institute of Technology, Atlanta, GA in 1977 and 1986, respectively.

He is currently a Professor of circuit theory and Chairman of the Department of Electronics at the Polytechnic of Turin. His research interests are in the field of electromagnetic compatibility, where he works on line modeling for signal integrity, field coupling to multiwire cables, and statistical methods in EMC. He also studied the interaction of electromagnetic radiation with biological systems, and the remote sensing of the atmosphere.

Dr. Canavero is the convener of the session on "Coupling to multiwire cables" of the URSI General Assembly (Kyoto, 1993 and Lille, 1996), and a member of the Italian delegation to NATO Sensor and Propagation Panel. He is also a member of the Italian Electrotechnical and Electronic Association (AEI) and of the IEEE EMC Society.

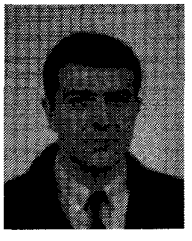

Bruno Dilecce was born in Barletta, Italy, on April 14, 1959. He received the electrical engineering degree and the Ph.D. degree in electrical sciences in 1983 and 1989, respectively, both from the University of Bari.

From 1983 to 1989, he worked at the University of Bari in the field of computer-aided analysis of electrical networks. Since 1989, he has been with the Electric System Department of Centro Ricerche FIAT, where he deals with automotive electrical systems. His main interests are in the areas of CAD/CAE tools for automotive electrical/electronic systems, electromagnetic compatibility, and circuit theory.